

# EXPERIMENTAL STUDY ON FLOW INTERACTION BETWEEN FORE- AND HINDWINGS OF DRAGONFLY IN HOVERING AND FORWARD FLIGHT

Hiroto Nagai\*, Koji Isogai\*, and Tatsumi Fujimoto\*  
 \*Nippon Bunri University

**Keywords:** *Flapping Wing, Unsteady Aerodynamics, Flow Visualization, Insect, Dragonfly*

## Abstract

There are various flow interactions between the fore- and hindwings of a dragonfly. However, the detailed mechanism of flow interaction between the fore- and hindwings has not been well understood. In this study, we clarify the aerodynamic mechanisms of flow interaction between fore- and hindwings of a dragonfly in hovering and forward flights. Measurements of unsteady aerodynamic forces acting on the tandem wings are conducted using a dynamically scaled mechanical model in a water tunnel. Moreover, flow visualization around the tandem wings is conducted using Particle Image Velocimetry. The effect of the phase difference between the fore- and hindwings on the aerodynamic characteristics is investigated in hovering and forward flights. The results indicate that the advanced hindwing ahead of the forewing, which is often used in steady flights of dragonflies, has a smaller variation with respect to the phase difference and a smaller difference between the fore- and hindwings in hovering and forward flight. In hovering flight, the flow interaction reduces the aerodynamic characteristics except at the phase difference of 0 deg. In forward flight, the advanced hindwing generates larger lift with a good efficiency than that without interaction

## 1 Introduction

A dragonfly has two pairs of fore- and hindwings and can move its wings independently. The motions of the four wings are controlled for various maneuvering. There are various flow interactions between the fore-

and hindwings in various flight conditions. Recent works have investigated the flow interactions between the fore- and the hind wings by means of experimental and numerical simulations [1–4]. However, the detailed mechanism of the flow interaction between the fore- and hindwings has not been well understood. In this study, we experimentally clarify the aerodynamic mechanisms of flow interaction between fore- and hindwings of a dragonfly in hovering and forward flight. Measurements of unsteady aerodynamic forces acting on the tandem wings are conducted using a dynamically scaled mechanical model in a water tunnel. In addition, flow visualization around the tandem wings is conducted using Particle Image Velocimetry (PIV). We investigate the effect of the phase difference between fore- and hindwings on the aerodynamic characteristics in hovering and forward flights.

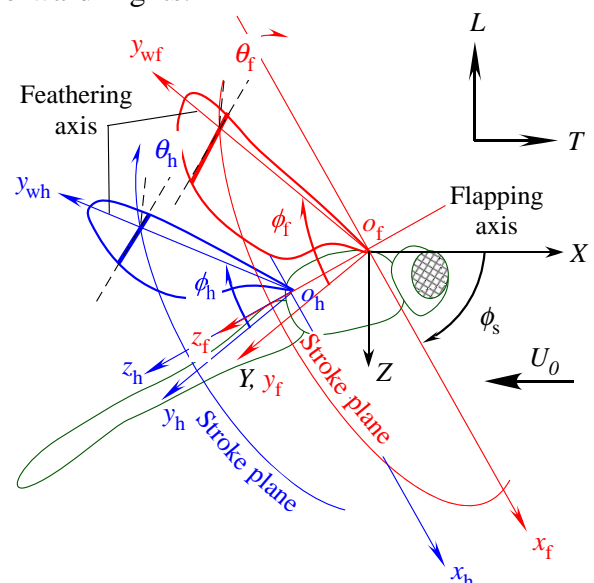


Fig. 1 3D-coordinate system of tandem wings.

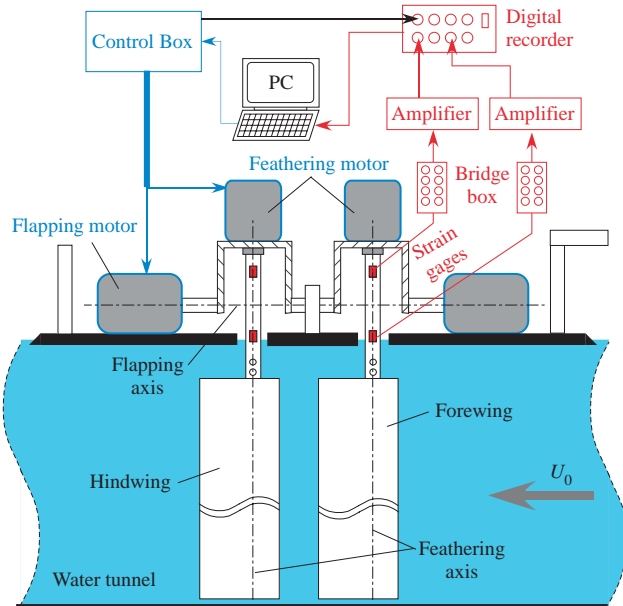
## 2 Experimental methods

Figure 1 shows the 3D coordinate system of tandem wings of a dragonfly. The wing kinematics of each wing consists of a flapping motion and a feathering motion. The time histories of the flapping angle  $\phi$  and the feathering angle  $\theta$  are represented as the sinusoidal functions, given by,

$$\begin{cases} \phi_f = \phi_{f0} \cos(2\pi t^*) \\ \theta_f = \theta_{f0} \cos(2\pi t^* + \xi_f) \end{cases}, \quad (1)$$

$$\begin{cases} \phi_h = \phi_{h0} \cos(2\pi t^* + \psi) \\ \theta_h = \theta_{h0} \cos(2\pi t^* + \psi + \xi_h) \end{cases}, \quad (2)$$

where  $\xi$  is the phase difference of the feathering motion ahead of the flapping motion,  $\psi$  is the phase difference between the fore- and the hindwing,  $t^*$  is the non-dimensional time based on a flapping cycle, the subscripts of f and h mean the fore- and the hindwings, respectively, and the subscript of 0 means an amplitude of angle. In this study, these parameters were determined based on the observed data of dragonflies [5], as follows:  $\phi_{f0} = 40$ ,  $\theta_{f0} = 60$ ,  $\phi_{h0} = 30$ ,  $\theta_{h0} = 45$ ,  $\xi_f = \xi_h = 90$  deg. The phase difference between the fore- and the hindwings  $\psi$  was varied with 45-deg increments from -180



**Fig. 2** Force measurement system and scaled mechanical apparatus.

to 180 deg. Note that the positive  $\psi$  means that the hindwing leads the forewing, and the negative  $\psi$  means that the forewing leads the hindwing. The stroke plane angle  $\phi_s$  was 0 deg in hovering flight and 45 deg in forward flight.

We used a dynamically scaled mechanical model of tandem wings for measurement of unsteady aerodynamic forces. The scaled mechanical apparatus and force measurement system are illustrated in Fig. 2. The flapping and feathering motions of the fore- and the hindwings were driven independently by four motors. The two test wings were made of aluminum and have the same rectangular planform (250 mm  $\times$  50 mm) with a thickness of 2 mm. The test wings were considered to be a rigid wing because its deformation was very small. The feathering axis of each wing is at 30% chord length. The distance of the feathering axes between the fore- and the hindwings was 65 mm, and the distance between the flapping axis and the wing base was 65 mm. Normal forces acting on the wings and flapping torques were measured using strain gages mounted on the shafts attached to the wing bases [6].

Flow similarity between a dragonfly and the scaled model was attained by agreements of the Reynolds numbers  $Re_f$ , the reduced frequencies  $k_f$ , and the advance ratio  $J$ , defined

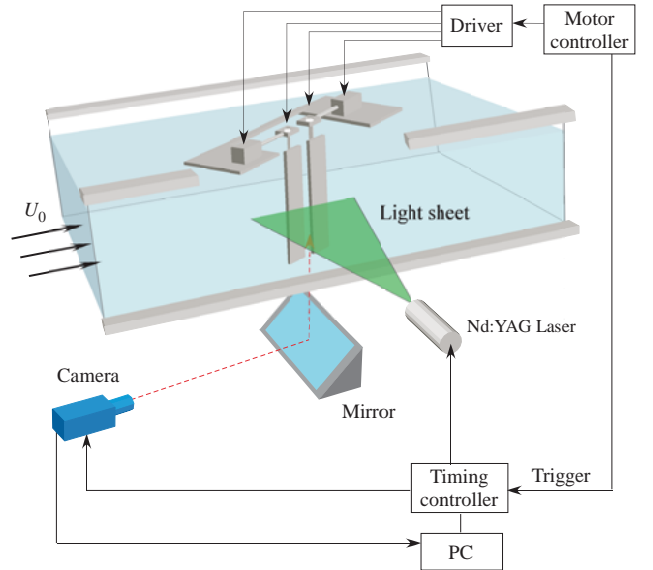


**Fig. 3** Particle Image Velocimetry (PIV) system.

by,

$$Re_f = V_{f0} b_f / \nu, \quad k_f = 2\pi f b_f / V_f, \quad J = U / V_{f0}, \quad (3)$$

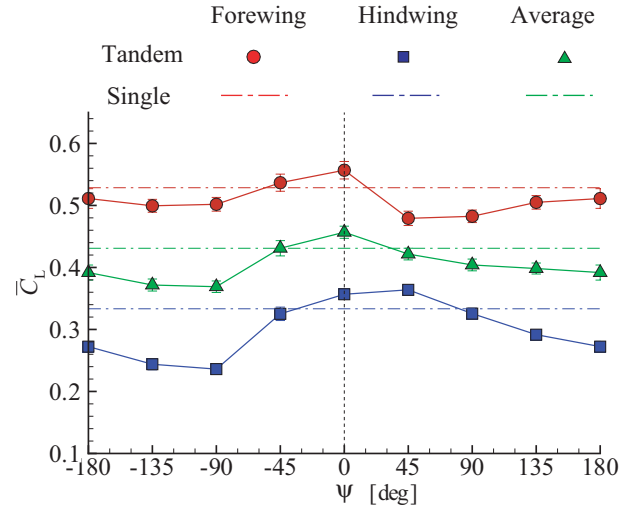
where  $b_f$  is the semi-chord length of the forewing,  $V_{f0}$  is the maximum flapping velocity of the forewing at 75% semi-span location,  $\nu$  is the kinematic viscosity of fluid,  $f$  is the flapping frequency, and  $U$  is the forward velocity. In our experiments, the Reynolds number is in 7000 – 11000, and the reduced frequency is 0.142. The advance ratio is 0 in the hovering flight and  $0 < J < 0.5$  in forward flight.

Flow visualization was conducted using 2D digital particle image velocimetry (DPIV). The DPIV measurement system is shown in Fig. 3. Although the same scaled mechanical apparatus as the force measurement was used, the test wings were different; those were a clear acrylic plate with a thickness of 4 mm so that a laser sheet can pass through the wings. Image acquisition and processing were performed by LaVision Davis 7.1 software. Image pairs were captured with a time interval of 3 ms when the flapping frequency is 0.2 Hz. To visualize the flow pattern of the entire wings, 2D PIV measurements were carried out by applying the laser sheet at 11 different heights [6].

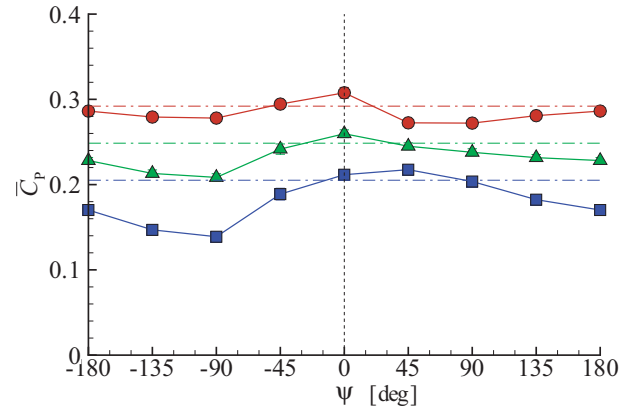
### 3 Results and Discussion in Hovering Flight

#### 3.1 Time-averaged aerodynamic characteristics

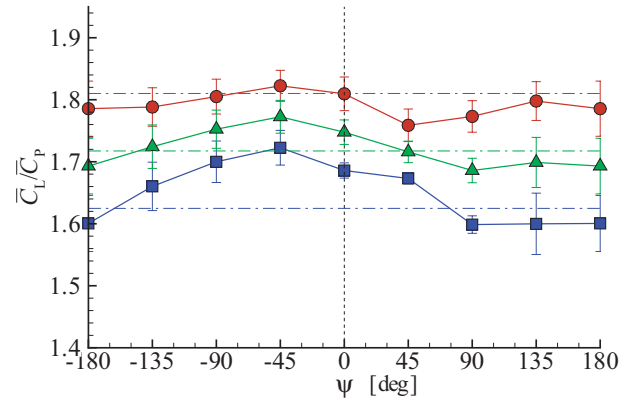
Unsteady aerodynamic forces in hovering flight were measured when the phase difference between the fore- and the hindwing  $\psi$  was varied from -180 to 180 deg. Measurements with a single wing were carried out for comparison. Figure 4 shows the time-averaged lift coefficient  $\bar{C}_L$ , power coefficient  $\bar{C}_p$ , and the efficiency of lift  $\bar{C}_L / \bar{C}_p$  with respect to  $\psi$ . From Fig. 4a,  $\bar{C}_L$  and  $\bar{C}_p$  of the forewing are larger than those of the hindwing. This is because the flapping amplitude of the forewing is larger than that of the hindwing.  $\bar{C}_L$  of the forewing is larger than that of the single forewing at  $\psi = -45$  and 0 deg and is the largest at  $\psi = 0$  deg. In the other range of  $\psi$ ,  $\bar{C}_L$  of the



a) Lift coefficient



b) Power coefficient



c) Efficiency of lift

**Fig. 4** Time-averaged aerodynamic characteristics in hovering flight with respect to the phase difference.

forewing is smaller than that of the single forewing and is the smallest at  $\psi = 45$  deg.

On the other hand,  $\bar{C}_L$  of the hindwing is larger than that of the single hindwing at  $\psi = 0$  and 45 deg and is the largest at  $\psi = 45$  deg. In the other range of  $\psi$ ,  $\bar{C}_L$  of the hindwing is smaller than that of the single hindwing. In particular,  $\bar{C}_L$  of the hindwing decreases rapidly in  $\psi = -180 - -90$  deg. The  $\bar{C}_L$  of the tandem wings (the average of the fore- and hindwings) is larger than that of the single wing (the average without interaction) at  $\psi = 0$  deg, while it is smaller in the other range of  $\psi$ . This result indicates that the flow interaction reduces the entire lift except for at  $\psi = 0$  deg, at which the lift of both wings are enhanced. The tendency of  $\bar{C}_p$  is similar to that of  $\bar{C}_L$  described above. The largest  $\bar{C}_L/\bar{C}_p$  appears at  $\psi = -45$  deg for both the fore- and hindwings.  $\bar{C}_L/\bar{C}_p$  of the forewing is smaller than that of the single forewing except at  $\psi = -45$  deg.  $\bar{C}_L/\bar{C}_p$  of the hindwing is larger than that of the single hindwing at  $\psi = -135 - 45$  deg.

On the basis of the observed data of a dragonfly [5] and our observation, the hindwing tends to lead the forewing in the steady flights, such as hovering and forward flight. On the other hand, our experimental results indicate that the forewing ahead of the hindwing ( $\psi < 0$ ) is better in terms of the efficiency of lift. In this case, however, there is a large difference of lift between the fore- and the hindwings and a large variation of lift with respect to  $\psi$ , as shown in Fig. 4a. These facts may make the flight control harder. On the other hand, the difference of lift and the variation of lift are small in the case of the hindwing ahead of the forewing ( $\psi > 0$ ). These results indicate that dragonflies may emphasize a good stability more than a good efficiency but with respect to the phase difference between the fore- and hindwings.

### 3.2 Time-histories of unsteady aerodynamic forces

To investigate the effects of the flow interaction on unsteady aerodynamic forces, we discuss the time histories of  $C_L$ . Figures 5a and 5b show the

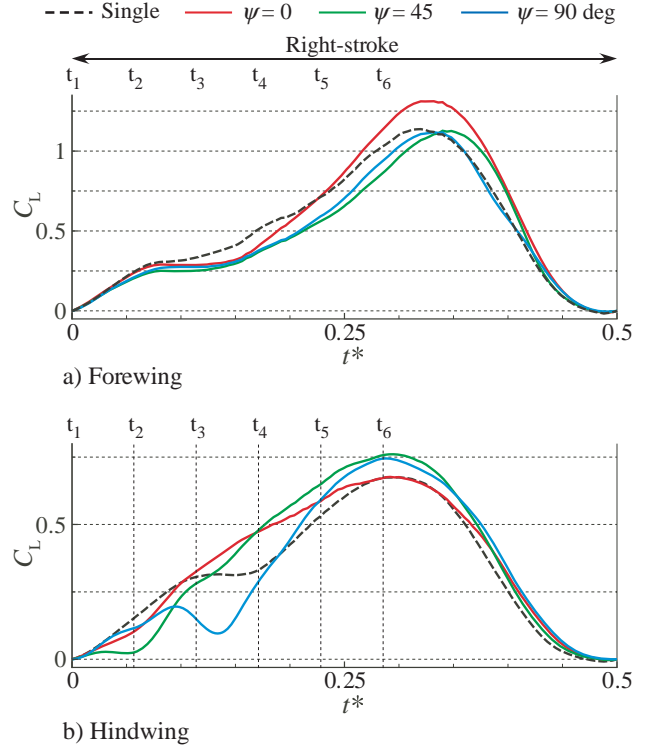


**Fig. 5** Time histories of lift coefficient in a right stroke in hovering flight.

time histories of  $C_L$  of the fore- and the hindwings, respectively, only during a right-stroke in the cases of the hindwing ahead of the forewing ( $\psi > 0$ ). In Fig. 5, note that each waveform is translated horizontally in order to match each flapping phase for comparison. From Fig. 5a, although the waveforms of  $C_L$  of the forewing are qualitatively similar, there are quantitative discrepancies. In the first half of the stroke ( $t^* = 0.0 - 0.25$ ),  $C_L$  in the tandem cases are smaller than that of the single forewing. This is attributed to the fact that the effective angle of attack of the forewing decreases due to the downwash induced behind the hindwing (see Fig. 6). In the last half of the stroke ( $t^* = 0.25 - 0.5$ ),  $C_L$  has a peak in every case. While the peaks of  $C_L$  at  $\psi = 45$  and 90 deg are the same as that of the single forewing, the peak at  $\psi = 0$  deg is larger than any other cases.

Next, let us focus on the waveform of  $C_L$  of the hindwing in Fig. 5b. There are qualitative and quantitative discrepancies among the phase differences, and between the single and tandem wings. In the case of  $\psi = 0$  deg,  $C_L$  is larger than that of the single hindwing at  $t^* = t_3 - t_4$ . In the

case of  $\psi = 45$  deg, while  $C_L$  is smaller than that of the single hindwing at  $t^* = t_2$ , it is larger at  $t^* = t_3 - t_6$  and have the larger peak. In the case of  $\psi = 90$  deg, while  $C_L$  has a rapid decline at  $t^* = t_2 - t_3$ , it is larger than that of the single hindwing at  $t^* = t_5 - t_6$  and has the larger peak.

### 3.3 Relation of aerodynamic force to flow pattern

We discuss the flow pattern measured by flow visualization, relating it with the aerodynamic force. Figure 6 shows the time histories of  $C_L$  and the corresponding sequences of flow pattern around the airfoil at 50% semi-span location in the cases of the tandem wings at  $\psi = 0, 45$ , and 90 deg in addition to the case of the single hindwing. In Fig. 6, the same subscript means that the hindwings are at the same flapping phase, and the subscripts of 1 – 6 correspond with  $t_1 - t_6$  in Fig. 5b.

First, let us focus on the flow pattern around the single hindwing without interaction (see Fig. 6a). At  $t^* = a_1$ , the wing is just at the reversal point; therefore, the flapping velocity is zero. In this moment, a starting vortex (SV) generated in the previous reversal point and a leading-edge vortex (LEV) generated through the previous stroke still remain. As shown in Fig. 6 a<sub>2</sub>, the feathering rotation under the influence of the remaining LEV causes a rotational vortex pair (RV) at both the leading- and the trailing-edges, which is called *wake capture effect* [7]. Next, at  $t^* = a_3 - a_4$ , while the shedding of a starting vortex from the trailing-edge causes a decrease of lift, the growth of a LEV causes an increase of lift; as a result, the lift keeps a constant value. At  $t^* = a_4 - a_6$ , the lift increases as the LEV grows. At  $t^* = a_6$ , the LEV begins to shed from the upper surface of the wing; then, the lift reaches a peak.

Next, let us focus on the flow pattern around the hindwing with interaction at  $\psi = 90$  deg (see Fig. 6b). At the beginning of the stroke ( $b_1 - b_2$ ), although there is a remaining LEV and a rotational vortex pair like Fig. 6a, these vortices are smaller than those in Fig. 6a. At  $t^* = b_3$ , since the hindwing is located under the forewing, it is affected by the downwash induced by the forewing. The downwash blows

off the vortices around the hindwing, which is shed from the trailing-edge as a starting vortex; then, the lift is reduced rapidly. At  $t^* = b_4$ ,  $C_L$  increases rapidly as a LEV grows. At  $t^* = b_5 - b_6$ ,  $C_L$  is larger than that of the single hindwing (see Fig. 5  $t_5 - t_6$ ). From Fig. 6  $b_5 - b_6$ , the LEV of the hindwing and the remaining LEV of the forewing form a vortex pair. The vortex pair with counter-rotating induces a downward jet flow between the vortex pair itself. The jet flow behind the hindwing causes the streamlines through the upper surface of the hindwing to curve downward; therefore, the lift of the hindwing is enhanced compared to the single hindwing.

Let us focus on the flow pattern around the hindwing with interaction at  $\psi = 45$  deg (see Fig. 6c). At  $t^* = c_1$ , a small remaining LEV is blown away downward by the downwash induced by the forewing because the hindwing is located under the forewing. At  $t^* = c_2$ , a small starting vortex is shed from the trailing-edge and blown away downstream by the downwash induced by the forewing; then,  $C_L$  is reduced slightly. At  $t^* = c_3$ , the remaining LEV around the forewing induces the strong downward flow behind the hindwing. That helps the separated flow from the leading-edge of the hindwing reattach on the upper surface; then, a strong LEV is formed on the upper surface, and  $C_L$  increases rapidly. At  $t^* = c_4 - c_6$ , the forewing is located upward and behind the hindwing. This position causes a strong downward flow between the fore- and hindwings. Therefore, since the streamlines through the upper of the hindwing curve downward,  $C_L$  of the hindwing increases.

Let us focus on the flow pattern around the hindwing with interaction at  $\psi = 0$  deg (see Fig. 6d). At  $t^* = d_1$ , the remaining LEV does not appear around the hindwing because it is blown away downward due to the downwash induced by the forewing. There is a downward flow in the left of the hindwing despite of the stroke reversal, when the effective angle of attack is almost zero. At the stroke reversal, the hindwing experiences a gradual variation of the relative flow velocity and the effective angle of attack because it is located under the downwash induced by the forewing. Therefore, any

noticeable starting vortex is not generated; as a result,  $C_L$  has no sudden dip and increases continuously in the early stroke. On the other hand, there is no flow in the left of the hindwing at the stroke reversal in the other cases ( $a_1$ ,  $b_1$ , and  $c_1$ ). Therefore, a large starting vortex is generated because the wing starts rapidly from the still fluid. At  $t^* = d_2$ , the LEV is already generated. It may be considered that the downwash induced by the forewing helps the separated flow from the leading-edge of the hindwing reattach on the upper surface. At  $t^* = d_3 - d_4$ , since the forewing catches up with the hind wing, the increment of  $C_L$  of the hindwing decreases.

Finally, let us focus on the forewing of  $\psi = 0$  deg (see Fig. 6d). At  $t^* = d_5$ , the forewing catches up with the hindwing.  $C_L$  of the forewing is larger than that of the single forewing when the forewing is located over the hindwing (see Fig. 5  $t_5$ ). This fact is similar to the wing-in-ground-effect.

#### 4 Results and Discussion in Forward Flight

Unsteady aerodynamic forces in forward flight were measured when the phase difference between the fore- and the hindwing  $\psi$  was varied from -180 to 180 deg in the range of the advance ratio,  $0 < J < 0.5$ . Measurements with a single wing were carried out for comparison. We focus on the aerodynamic characteristics at  $J = 0.25$ , the medium forward speed for dragonflies. Figure 7 shows the time-averaged lift coefficient  $\bar{C}_L$ , thrust coefficient  $\bar{C}_T$ , power coefficient  $\bar{C}_P$ , the efficiency of lift  $\bar{C}_L/\bar{C}_P$ , the propulsive efficiency  $\eta (= \bar{T}U/\bar{P})$  with respect to  $\psi$ .

From Fig. 7a,  $\bar{C}_L$  of the forewing is smaller than that of the single forewing except at  $\psi = -45$  and 0 deg.  $\bar{C}_L$  of the hindwing is much larger than that of the single hindwing at  $\psi = -45 - 180$  deg and much smaller at  $\psi = -90$  and -135 deg. The average  $\bar{C}_L$  of the tandem wings is larger than that of the single wing at  $\psi = -45 - 135$  deg and smaller at  $\psi = -180 - 90$  deg. In Fig. 7c,  $\bar{C}_P$  has a similar tendency to  $\bar{C}_L$

described above although the variation of  $\bar{C}_P$  is small. In Fig. 7d,  $\bar{C}_L/\bar{C}_P$  of the forewing is smaller than that of the single wing at all the phase difference. On the other hand,  $\bar{C}_L/\bar{C}_P$  of the hindwing is much larger than that of the single hindwing at  $\psi = -45 - 180$  deg while it is smaller at  $\psi = -90$  and -135 deg. The average  $\bar{C}_L/\bar{C}_P$  of the tandem wings are larger than that without interaction at  $\psi = -90$  and -135 deg. These results indicate that the positive  $\psi$ , when the hindwing leads the forewing, generates a larger lift and has a better efficiency of lift, unlike in hovering flight. In addition, the variation of lift with respect to  $\psi$  and the difference of lift between the fore- and hindwings are small in the range of the positive  $\psi$  compared to the negative  $\psi$ . Therefore, the positive  $\psi$  generates larger lift with a good efficiency and has a good stability in forward flight.

From Fig. 7b, the variations of  $\bar{C}_T$  is small with respect to  $\psi$ .  $\bar{C}_T$  of the forewing is almost the same as that of the single forewing except at  $\psi = 0$  and 180 deg, at which the forewing is under the wing-in-ground-effect.  $\bar{C}_T$  of the hindwing is smaller than that of the single hindwing at all  $\psi$ . The average  $\bar{C}_T$  of the tandem wings is smaller than that without interaction. The propulsive efficiency  $\eta$  of the forewing is almost the same as that of the single forewing.  $\eta$  of the hindwing is smaller than that of the single hindwing except at  $\psi = -90$  deg. Therefore, the average  $\eta$  of the tandem wings is smaller than that of the hindwing except at  $\psi = -90$  deg.

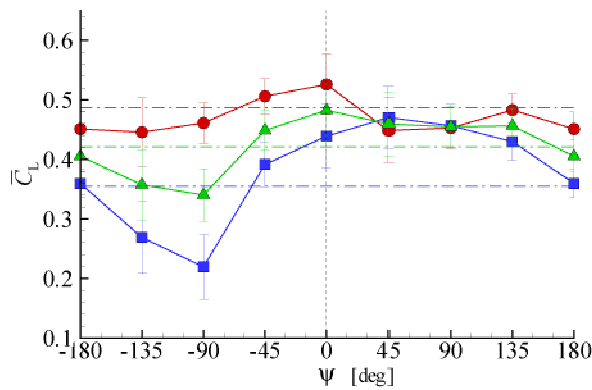
In forward flapping flight, the wings experience a larger relative inflow velocity in the down-stroke and a smaller velocity in the up-stroke because of the forward velocity. The lift is generated mainly in the down-stroke, and the thrust is in the up-stroke because of the inclined stroke plane angle. The advanced forewing cuts off the supply of the forward velocity to the hindwing. Therefore, the hindwing can not benefit from the forward velocity in this case. On the other hand, the advanced hindwing can benefit from the

## EXPERIMENTAL STUDY ON FLOW INTERACTION BETWEEN FORE- AND HINDWINGS OF DRAGONFLY IN HOVERING AND FORWARD FLIGHT

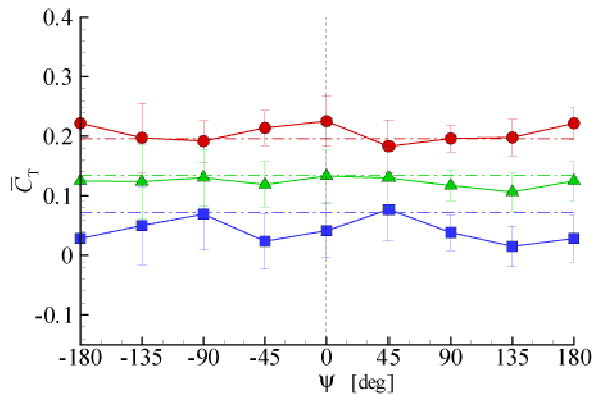
forward velocity without the interruption of the forewing. Moreover, the advanced hindwing in the down-stroke also benefits from the downwash induced by the delayed forewing in the up-stroke. As a result, the advanced hindwing generates larger lift than that without interaction.

### 5 Conclusions

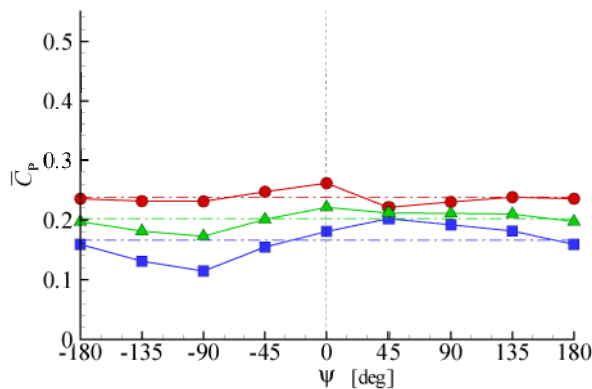
We have experimentally investigated the effect of the phase difference between the fore- and hindwings on the aerodynamic characteristics in hovering and forward flight. The results indicate that the advanced hindwing ahead of the forewing, which is often used in steady flights of dragonflies, has the smaller variation with respect to the phase difference  $\psi$  and the smaller



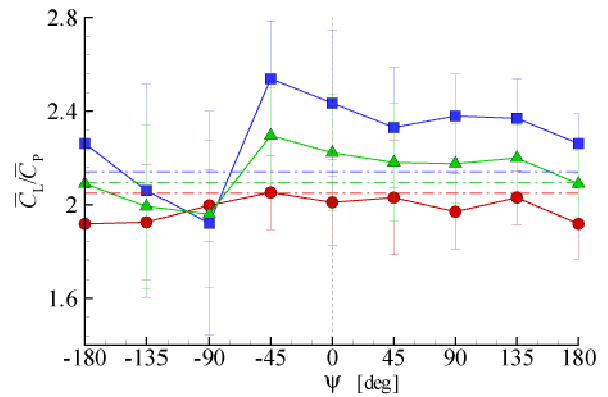
a) Lift coefficient



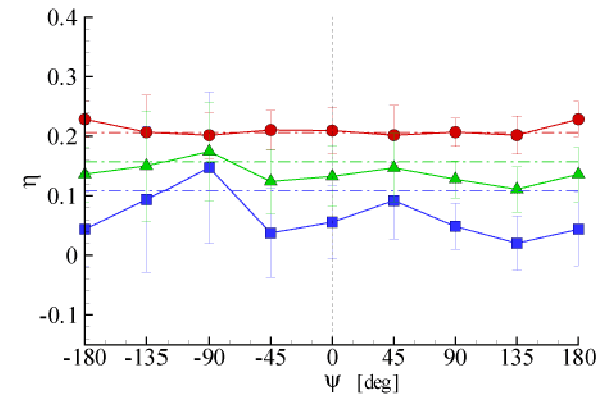
b) Thrust coefficient



c) Power coefficient



d) Efficiency of lift



e) Propulsive efficiency



**Fig. 7** Time-averaged aerodynamic characteristics with respect to the phase difference in forward flight of  $J = 0.25$  at  $\psi = 45$  deg.

difference between the fore- and hindwings. This fact may contribute to the flight stability of a dragonfly. In hovering flight, the flow interaction between the fore- and hindwing reduces the aerodynamic characteristics except at  $\psi = 0$  deg, at which the wings experience the wing-in-ground-effect. In forward flight, the advanced hindwing generates larger lift with a good efficiency because of the benefits from the forward velocity without interruption of the forewing and from the downwash induced by the forewing. Therefore, the flow interaction with the advanced hindwing is more effective in forward flight.

*Symposium on Aerospace Engineering*, Cheju, Korea, pp. 133–140, 2008.

### Copyright Statement

The authors confirm that they, and/or their company or organization, hold copyright on all of the original material included in this paper. The authors also confirm that they have obtained permission, from the copyright holder of any third party material included in this paper, to publish it as part of their paper. The authors confirm that they give permission, or have obtained permission from the copyright holder of this paper, for the publication and distribution of this paper as part of the ICAS2010 proceedings or as individual off-prints from the proceedings.

### Acknowledgement

Authors acknowledge the support of Ministry of Education, Culture, Sports, Science and Technology of Japan under the High-Tech Research Center Promotion Program. The authors express their great appreciation to Akihiro Nishi and Ryo Yamaji for their help in experiments.

### References

- [1] Yamamoto M and Isogai K. Measurement of unsteady fluid dynamic forces for a mechanical dragonfly model. *AIAA Journal*, Vol. 43, No. 12, pp. 2475–2480, 2005.
- [2] Lehmann F –O, Sane S P and Dickinson M H. The aerodynamic effects of wing-wing interaction in flapping insect wings. *J. Exp. Biol.*, 208, pp. 3075–3092, 2005.
- [3] Sun M and Lan S. A computational study of the aerodynamic forces and power requirements of dragonfly (*Aeschna juncea*) hovering. *J. Exp. Biol.*, 207, pp. 1887–1901, 2004.
- [4] Wang J K. and Sun M. A computational study of the aerodynamics and forewing-hindwing interaction of a model dragonfly in forward flight. *J. Exp. Biol.*, 208, pp. 3785–3804, 2005.
- [5] Azuma A and Watanabe T. Flight performance of a dragonfly. *J. Exp. Biol.*, 137, pp. 221–252, 1988.
- [6] Nagai H, Isogai K, Fujimoto T and Hayase T. Experimental and numerical study of forward flight aerodynamics of insect flapping wing. *AIAA Journal*, Vol. 47, No. 3, pp. 730–742, 2009.
- [7] Nagai H, Isogai K and Fujimoto T. Experimental study of wing-wake interactions of insect flapping wing. *Proc. KSAS-JSASS Joint International*

**EXPERIMENTAL STUDY ON FLOW INTERACTION BETWEEN FORE- AND HINDWINGS OF DRAGONFLY IN HOVERING AND FORWARD FLIGHT**

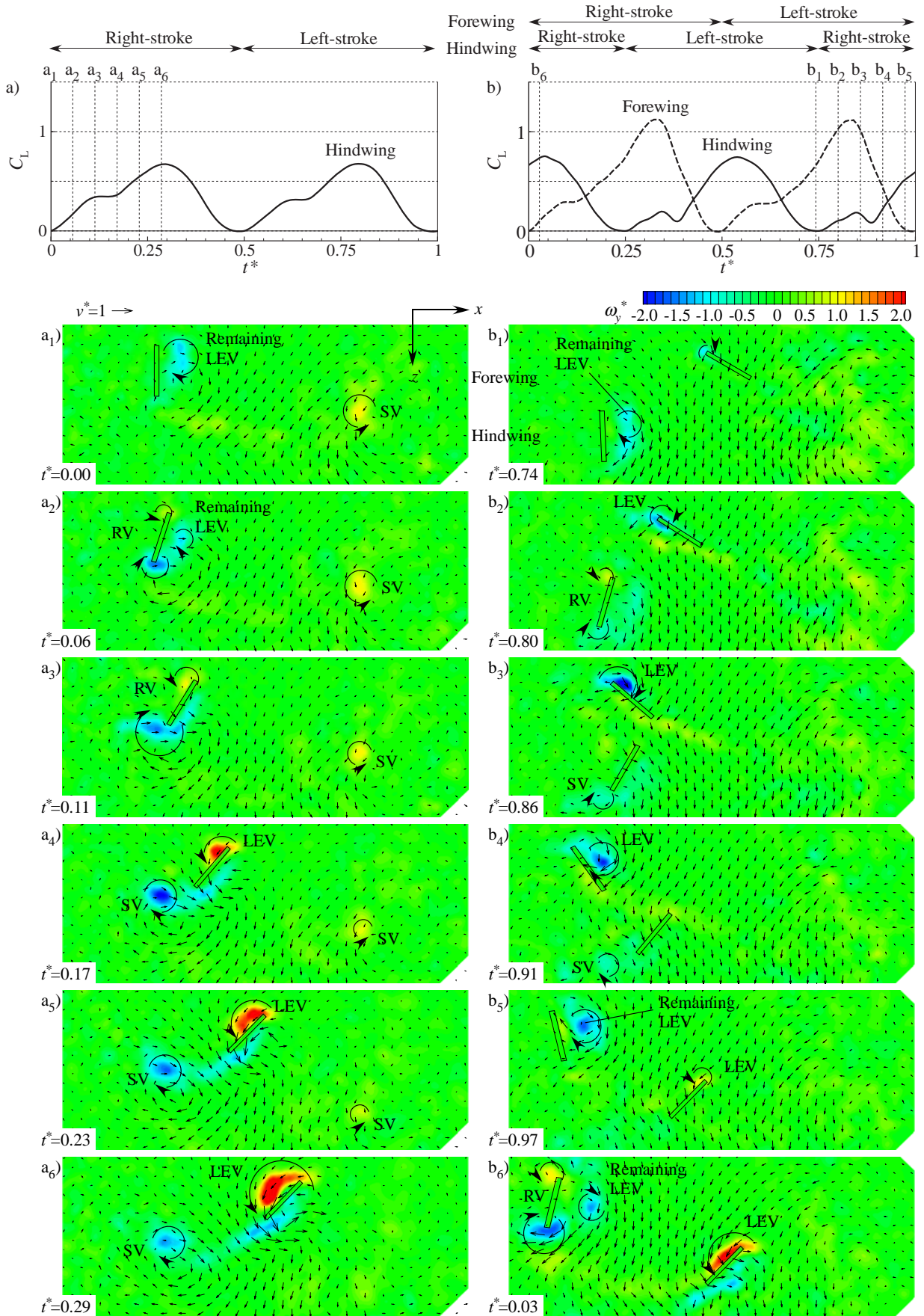


**Fig. 6** Time histories of lift coefficient and the corresponding flow patterns around the airfoils at 50% semi-span location: a) single hindwing, b) tandem wings at  $\psi = 90$  deg.

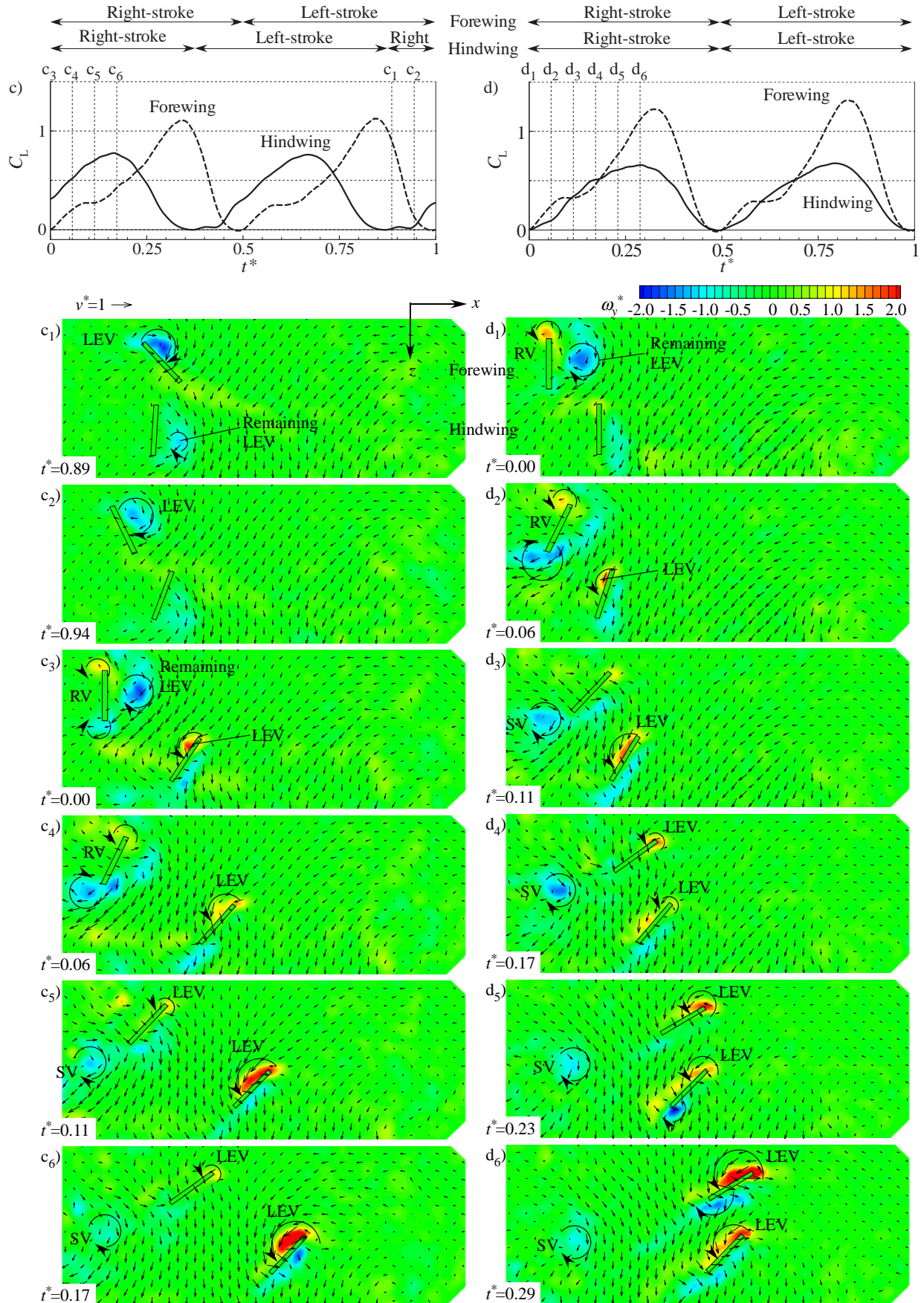


**Fig. 6** Time histories of lift coefficient and the corresponding flow patterns around the airfoils at 50% semi-span location: c) tandem wings at  $\psi = 45$  deg, b) tandem wings at  $\psi = 0$  deg.